Figure S1

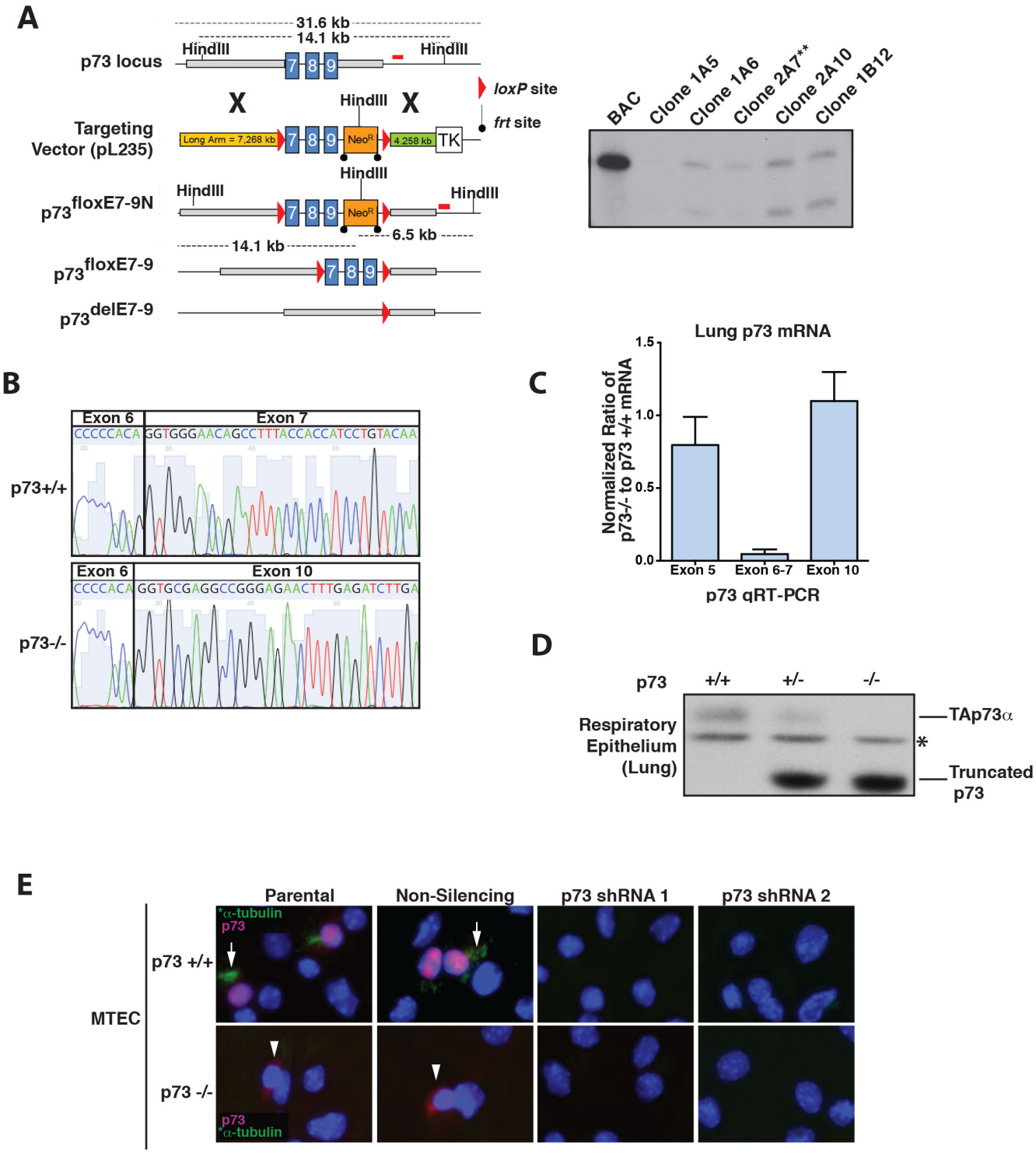
A
31.6 kb
14.1 kb
HindIII
HindIII
p73 locus
7 8 9
loxP site
frt site
X
HindIII
X
Targeting Vector (pL235)
Long Arm = 7,268 kb
7 8 9
NeoR
4.258 kb
TK
HindIII
p73floxE7-9N
HindIII
HindIII
7 8 9
NeoR
6.5 kb
14.1 kb
p73floxE7-9
7 8 9
p73delE7-9
BAC
Clone 1A5
Clone 1A6
Clone 2A7**
Clone 2A10
Clone 1B12
B
Exon 6
Exon 7
CCCCCACA GGTGGGAACAGCCTTTACCACCATCCTGTACAA
p73+/+
Exon 6
Exon 10
CCCCACA GGTGCGAGGCCGGGAGAACTTTGAGATCTTGA
p73-/-
C
Lung p73 mRNA
Normalized Ratio of p73-/- to p73 +/+ mRNA
1.5
1.0
0.5
0.0
Exon 5
Exon 6-7
Exon 10
p73 qRT-PCR
D
p73
+/+
+/-
-/-
Respiratory Epithelium (Lung)
TAp73α
*
Truncated p73
E
Parental
Non-Silencing
p73 shRNA 1
p73 shRNA 2
MTEC
p73 +/+
*α-tubulin
p73
p73 -/-
p73
*α-tubulin

Figure S2

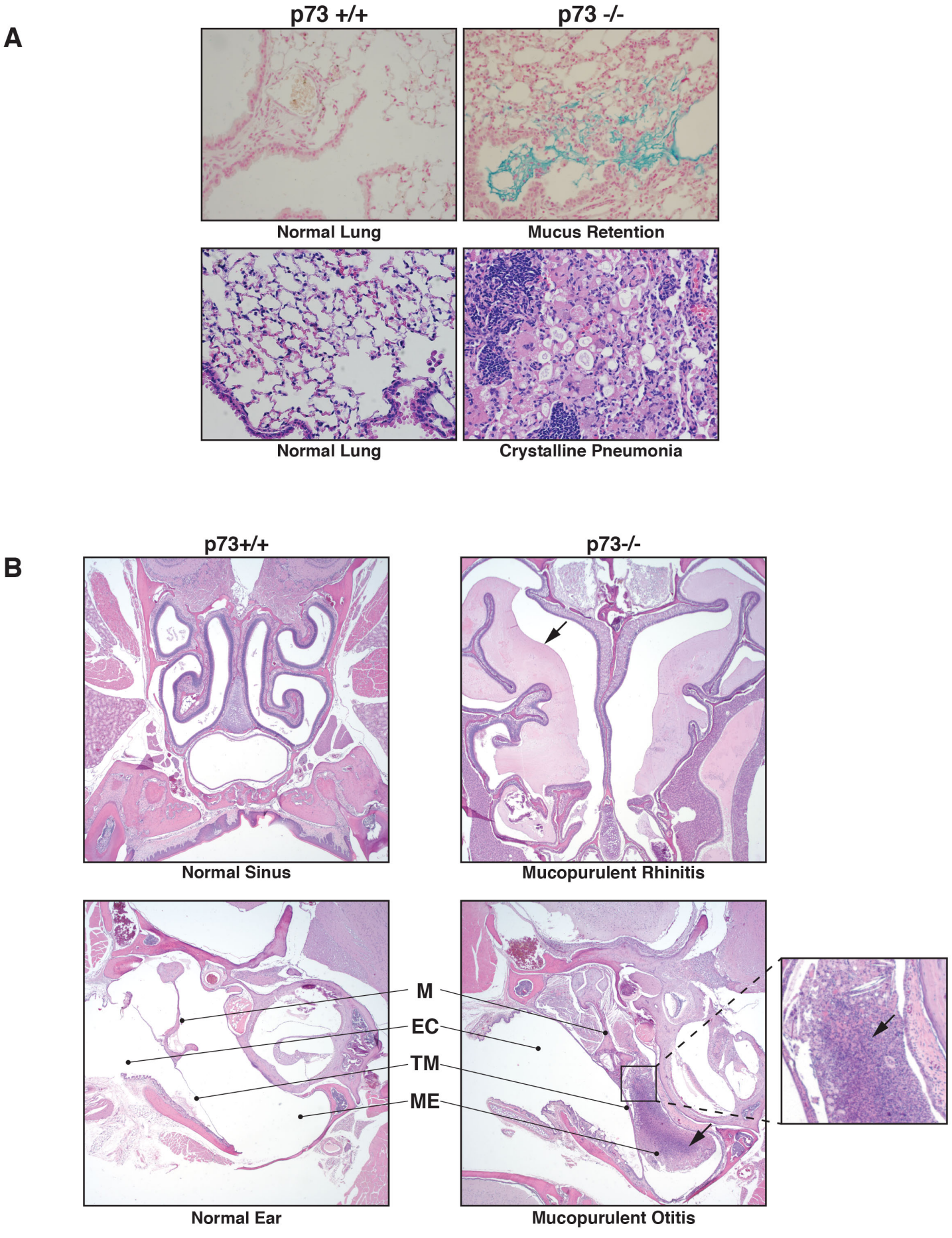
A
p73 +/+
p73 -/-
Normal Lung
Mucus Retention
Normal Lung
Crystalline Pneumonia
B
p73+/+
p73-/-
Normal Sinus
Mucopurulent Rhinitis
M
EC
TM
ME
Normal Ear
Mucopurulent Otitis

Figure S3

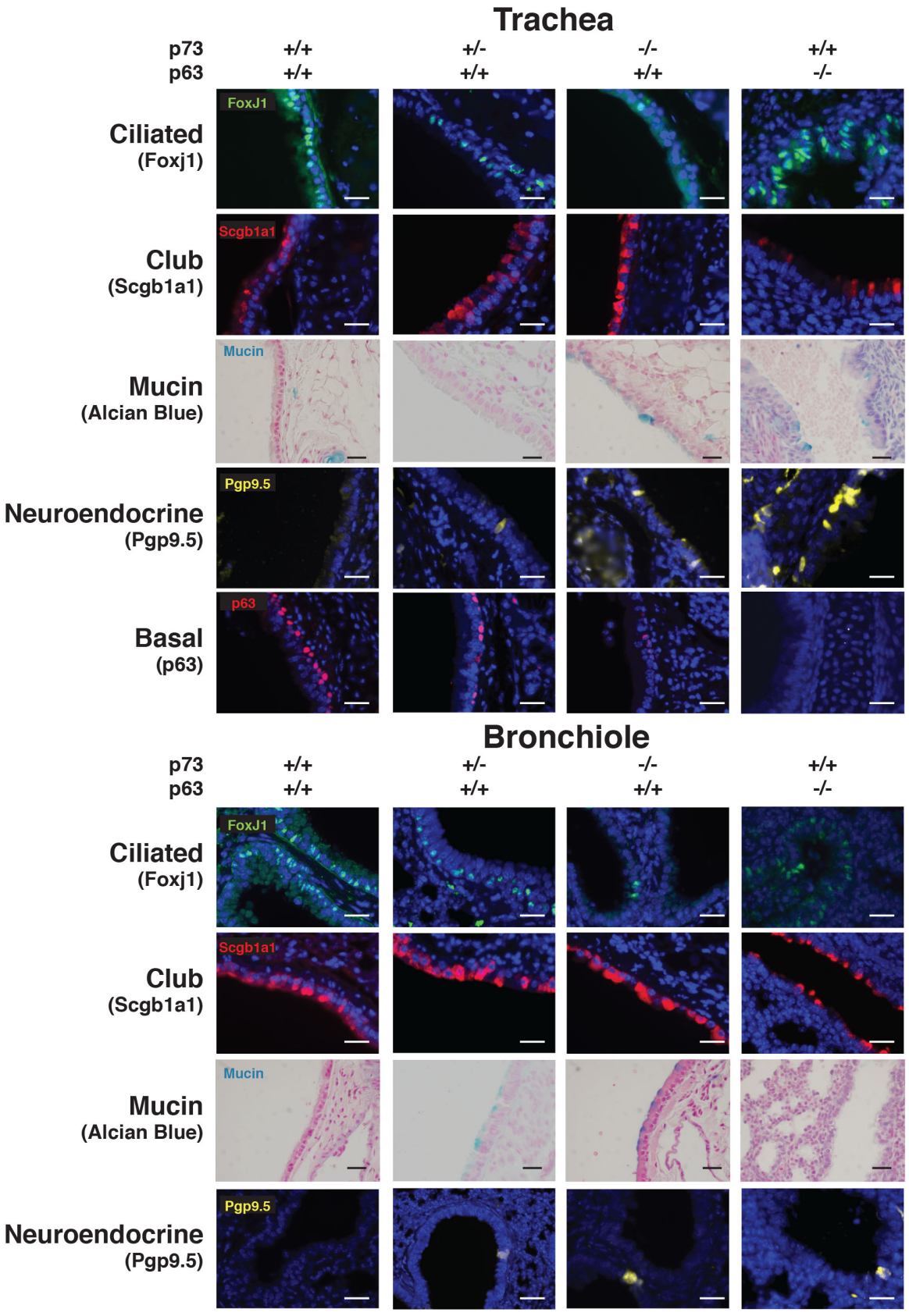
Trachea
p73 +/+ +/- -/- +/+
p63 +/+ +/+ +/+ -/-
Ciliated (Foxj1)
FoxJ1
Club (Scgb1a1)
Scgb1a1
Mucin (Alcian Blue)
Mucin
Neuroendocrine (Pgp9.5)
Pgp9.5
Basal (p63)
p63
Bronchiole
p73 +/+ +/- -/- +/+
p63 +/+ +/+ +/+ -/-
Ciliated (Foxj1)
FoxJ1
Club (Scgb1a1)
Scgb1a1
Mucin (Alcian Blue)
Mucin
Neuroendocrine (Pgp9.5)
Pgp9.5

Figure S4

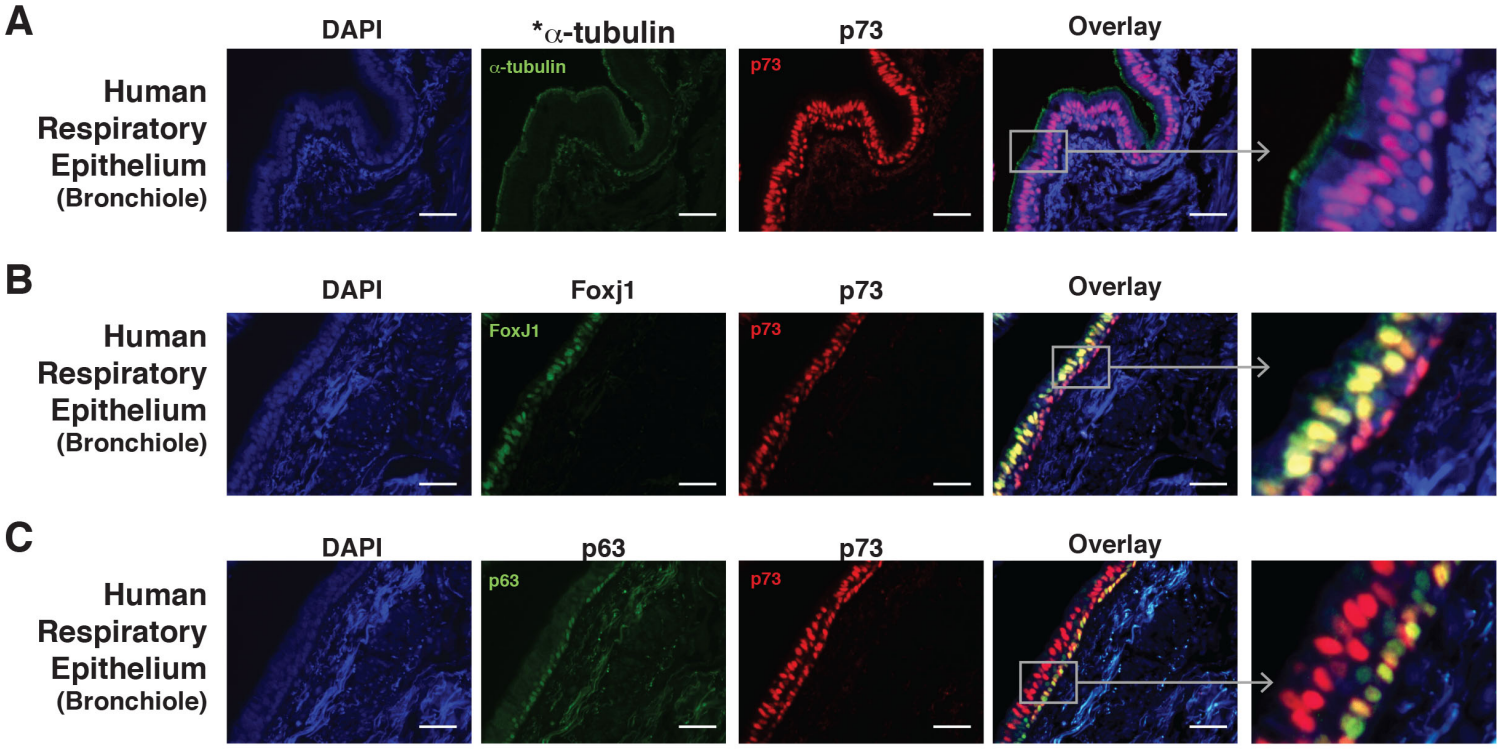
A
DAPI
*α-tubulin
p73
Overlay
Human Respiratory Epithelium (Bronchiole)
α-tubulin
p73
B
DAPI
Foxj1
p73
Overlay
Human Respiratory Epithelium (Bronchiole)
FoxJ1
p73
C
DAPI
p63
p73
Overlay
Human Respiratory Epithelium (Bronchiole)
p63
p73

Figure S5

A

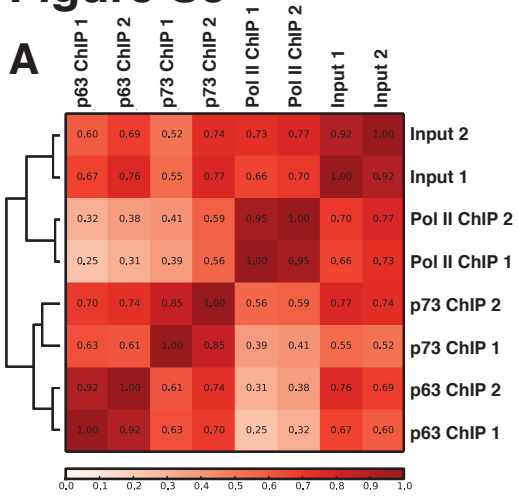

B

Sample	Number of Binding Sites	Median Distance to Nearest TSS (bp)
Pol II ChIP	53,684	1,484
p73 ChIP	1,767	9,531
p63 ChIP	3,861	12,810

C

	Analysis of the Genomic Binding Sites								
	p73			p63			Pol II		
	# of Peaks	Log Ratio Enrichment	P-value	# of Peaks	Log Ratio Enrichment	P-value	# of Peaks	Log Ratio Enrichment	P-value
Promoters	259	2.11	1.02E-114	127	0.75	4.06E-13	16943	3.14	0.00E+00
CpG Island	175	2.52	3.48E-83	59	1.19	6.30E-16	14635	3.93	0.00E+00
UTR 5'	151	2.58	3.86E-38	33	0.7	1.10E-02	11795	3.95	0.00E+00
Exons	217	0.53	8.31E-07	204	0.22	3.26E-03	18323	1.95	0.00E+00
TTS	37	0.19	2.15E-01	63	-0.01	4.91E-01	4889	1.85	0.00E+00
Coding	85	-0.05	3.89E-01	123	0.14	1.29E-01	10425	1.5	0.00E+00
UTR 3'	18	-0.12	3.45E-01	62	0.23	5.37E-02	2735	1.19	0.00E+00
Introns	791	-0.07	2.41E-03	1928	0.04	7.05E-03	25776	-0.26	0.00E+00
Intergenic	730	-0.66	0.00E+00	1740	-0.62	0.00E+00	13864	-1.37	0.00E+00

D

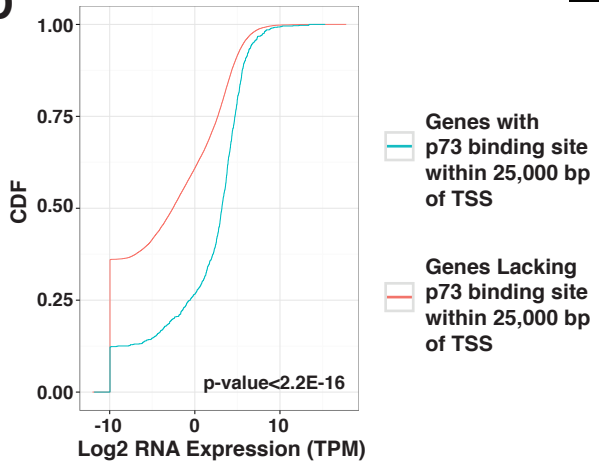

E

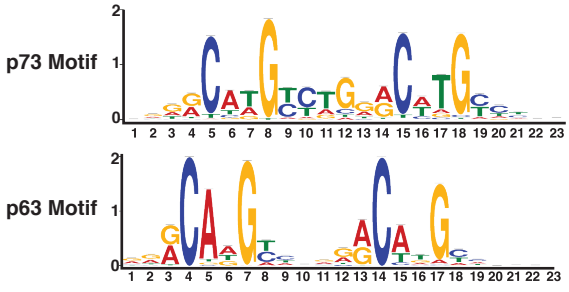

F

Representative Genes Previously Reported as p73 Target Genes			
Gene Symbol	q-value	Distance (bp) from TSS	Overlapping p63 Binding
Mdm2	7.9433E-46	-7,029	
	1.2589E-16	-15	✓
Cdkn1a	1.5849E-27	-11,938	✓
	1E-12	740	
	1E-09	-9	

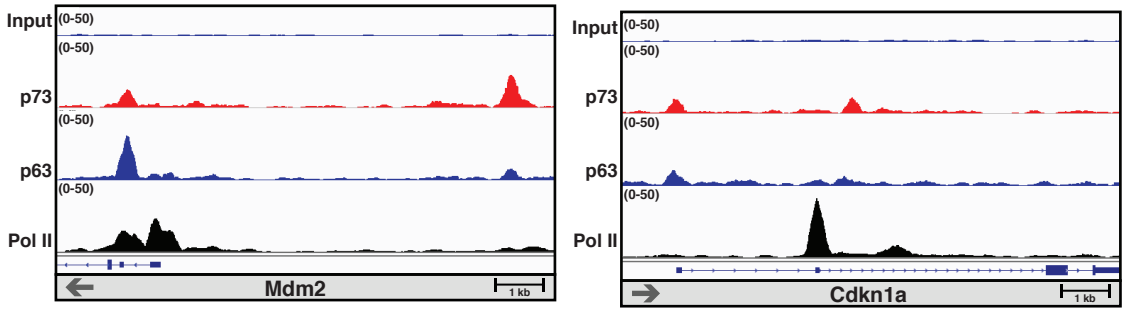

Figure S6

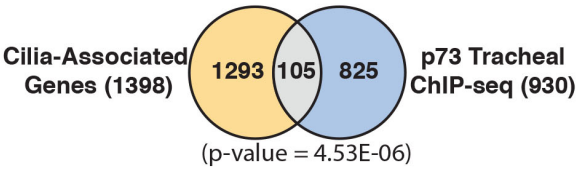

Overlap of Cilia-Associated Gene Set and p73 ChIP-seq			
Gene Symbol	q-value	Distance (bp) from TSS	Overlapping p63 Binding
Traf3ip1	7.9433E-123	-4,151	✔
4833427G06Rik	5.0119E-114	-3,895	✔
Hs6st2	1.9953E-110	8,582	✔
Rbl2	1.2589E-107	12,036	✔
Foxj1	1.5849E-103	8,146	✔
Cct4	6.30957E-96	-1,122	✔
Ercc3	1E-92	20,031	
Spata18	3.16228E-84	-1,498	
Lztfl1	1.99526E-75	5,409	
Glipr1	3.98107E-75	-209	
Usp2	2.51189E-72	-180	✔
Slc38a6	1.25893E-70	8,104	✔
6430531B16Rik	5.01187E-69	8,233	✔
Rgs3	6.30957E-69	2,338	✔
Slc25a17	3.16228E-68	3,624	✔
Myb	5.01187E-67	4,187	✔
Trp73	1.58489E-64	-8,719	✔
Gm684	5.01187E-57	9,498	✔
Zfp51	3.98107E-50	-11,405	
Ccdc113	1.58489E-47	13,738	
Trit1	2.51189E-46	-2,229	✔
Gnpnat1	1.25893E-45	-17,281	
Stk33	3.98107E-45	3,531	
Glis3	5.01187E-42	22,548	✔
Fam161a	6.30957E-40	-16	✔
Tp73	1.25893E-39	-161	
Exo1	7.94328E-38	-4,782	
Cyp2s1	7.94328E-38	-2,1047	✔
Tubb4b	3.98107E-37	-767	✔
Foxj1	5.01187E-37	5,006	✔
Dcdc2a	1.58489E-36	-24,669	
Aox1	6.30957E-35	22,462	
Ppil6	1.25893E-32	814	✔
Wdr38	1.58489E-32	-9,073	✔
Sirt3	3.16228E-32	558	
Cyp2s1	2.51189E-31	-15,181	✔
Pex3	5.01187E-31	-39	
Banp	6.30957E-28	303	
Fxn	3.16228E-26	10,028	✔
Mtg1	3.16228E-26	-17	
Cmbl	1.25893E-25	1,029	✔
Ankrd10	3.16228E-22	-8,753	
Arc	6.30957E-21	6,716	
Tmem57	2.51189E-20	-2,702	
Zfp667	5.01187E-20	-1,941	
Spag16	1E-19	2,678	
Stx16	6.30957E-19	-46	✔
Tiam1	3.98107E-18	-15,934	✔
Hipk1	5.01187E-18	-19,180	
2310007B03Rik	5.01187E-18	7	✔
Atp6v1h	1E-17	20,715	✔
Krr1	1.99526E-17	29	
Sec24b	1E-16	6,221	✔
Megf6	3.98107E-16	10,490	✔
Rbm34	1E-15	-27	
Mphosph10	1.99526E-15	-20	

Overlap of Cilia-Associated Gene Set and p73 ChIP-seq			
Gene Symbol	q-value	Distance (bp) from TSS	Overlapping p63 Binding
Rrp15	1.99526E-15	-26	
Tmem101	1.99526E-15	-22	
Pih1d2	3.98107E-15	-7	
Hdac8	1.25893E-14	23,315	✔
Lgals12	1.58489E-14	23,839	✔
Eps8	1.99526E-13	-537	✔
Med12l	1.99526E-13	-15,360	
Pla2g16	3.16228E-13	-4,289	
Edc4	5.01187E-13	-23	
Cep135	1.58489E-12	411	
Ugt1a6a	1.58489E-12	-192	✔
Mrpl39	5.01187E-12	-61	
Dnaic1	6.30957E-12	-3,120	
Rel	1.25893E-11	189	
Pepd	1.99526E-11	4,566	
Tmem69	3.16228E-11	-45	
Man2c1	5.01187E-11	55	
Sord	1.25893E-10	-3,167	✔
Psmf1	1.58489E-10	-53	
Alkbh3	1.99526E-10	-42	
Gapvd1	6.30957E-10	987	
Riiad1	7.94328E-10	3,844	✔
Ap3m2	0.000000001	-5,110	✔
Ccdc17	0.000000001	-45	✔
Foxj1	1.25893E-09	5,828	✔
Dnaic2	1.99526E-09	-24,855	✔
Rfx3	2.51189E-09	-13,813	
Jag1	6.30957E-09	8,416	✔
1110004E09Rik	7.94328E-09	-26	
B230118H07Rik	1.25893E-08	-961	
Anxa8	3.16228E-08	-148	
2610028H24Rik	3.98107E-08	-1,709	
Golga3	5.01187E-08	-54	
Nhsl1	7.94328E-08	-19,948	
1700001C02Rik	7.94328E-08	1596	
Ect2	1.58489E-07	11,005	✔
Cryaa	2.51189E-07	8,583	✔
Faf2	2.51189E-07	7,552	✔
2700049A03Rik	2.51189E-07	208	
Bms1	5.01187E-07	3	
Entpd5	7.94328E-07	482	✔
Slc25a17	0.000001	3,919	✔
Dgcr6	1.25893E-06	4,841	
Dpcd	1.58489E-06	5,594	
Lrpprc	1.58489E-06	2,588	
Slc47a2	1.58489E-06	22,724	
Slc35b1	1.99526E-06	3,663	✔
Dpagt1	1.99526E-06	-31	
Mettl15	7.94328E-06	-32	
Mllt10	0.00001	-7,089	✔
Nek2	3.16228E-05	-1,283	
Glipr1	6.30957E-05	549	
Ces1b	6.30957E-05	-222	✔
B230118H07Rik	6.30957E-05	-82	
Tnpo3	6.30957E-05	77	
Rcbtb2	0.000199526	-12,004	✔

***Gray highlighting indicates genes that were differentially expressed after ectopic overexpression of p73 in either p73+/+ and/or p73-/- MTEC cultures**

Table S1. Quantification of Epithelial Cells within Pulmonary Epithelium

	Trachea					Bronchiole			
	Number of the indicated type cells / Total number of all cells lining the respiratory epithelium in a field of view					Number of the indicated type cells / Total number of all cells lining the respiratory epithelium in a field of view			
Genotype	**Neuroendocrine**	**Mucin**	**Ciliated**	**Club**	**Basal**	**Neuroendocrine**	**Mucin**	**Ciliated**	**Club**
p73+/+	4 / 98	0 / 101	16 / 46	15 / 61	18 / 60	0 / 48	0 / 52	36 / 92	19 / 38
	0 / 67	0 / 94	23 / 57	20 / 76	10 / 46	6 / 130	1 / 31	36 / 129	22 / 40
	13 / 110	0 / 82	7 / 19	16 / 39	21 / 90	3 / 106	2 / 49	30 / 90	22 / 31
	0 / 98	0 / 84	14 / 32	12 / 50	12 / 48	7 / 67	0 / 44	26 / 81	36 / 57
	0 / 104	2 / 112	22 / 47	18 / 72	14 / 50	0 / 66	2 / 32	22 / 94	32 / 48
	0 / 71	0 / 91	13 / 37	26 / 97	13 / 54	0 / 55	0 / 62	25 / 72	39 / 70
	2 / 81	0 / 77	13 / 39	17 / 71	9 / 41	3 / 76	0 / 58	26 / 91	35 / 51
	1 / 46	3 / 210	20 / 54	13 / 62	12 / 42	0 / 48	0 / 80	27 / 86	19 / 32
	0 / 58	5 / 167	22 / 41	16 / 42	12 / 46	4 / 80	3 / 63	18 / 46	42 / 60
	0 / 67	3 / 121	18 / 58	18 / 44	13 / 39	0 / 113	2 / 60	10 / 56	45 / 60
	0 / 93	1 / 76	18 / 45	15 / 34	13 / 36	0 / 89	1 / 73	9 / 30	20 / 31
	0 / 66	3 / 141	15 / 44	12 / 39	10 / 36	0 / 118	4 / 64	9 / 26	26 / 43
	2 / 89	2 / 76	24 / 63	20 / 70	21 / 65	0 / 75	0 / 72	19 / 60	20 / 32
	1 / 46	2 / 78	20 / 48	12 / 39	11 / 31	7 / 84	0 / 43	15 / 44	28 / 42
	0 / 67	0 / 132	27 / 74	14 / 52	12 / 45	0 / 124	0 / 31	10 / 34	28 / 40
	0 / 102	0 / 104	25 / 68	20 / 60	16 / 35	0 / 90	3 / 88	10 / 38	79 / 90
	0 / 57	5 / 86	22 / 60	12 / 49	19 / 64	2 / 55	0 / 59	33 / 89	49 / 63
	0 / 86	0 / 79	24 / 66	15 / 50	23 / 72	0 / 46	1 / 47	12 / 31	35 / 53
	2 / 91	6 / 134	15 / 53	56 / 118	20 / 71	0 / 53	0 / 51	8 / 41	38 / 57
	1 / 49	18 / 213	19 / 51	14 / 47	25 / 86	3 / 85	5 / 87	10 / 71	38 / 51
	0 / 51	0 / 95	19 / 61	9 / 27	12 / 38	0 / 62	2 / 31	12 / 40	39 / 75
	1 / 65	0 / 134	18 / 54	11 / 37	14 / 51	0 / 69	0 / 64	15 / 64	43 / 63
	2 / 53	0 / 92	11 / 49	27 / 94	18 / 61	0 / 72	1 / 57	12 / 52	41 / 52
	1 / 52	0 / 145	42 / 140	23 / 62	12 / 39	0 / 91	2 / 78	15 / 54	23 / 35
Average % Positive	1.5	1.5	36.5	31.1	29.3	1.8	2.1	29.5	66.5
Standard Deviation	2.6	2.2	6.3	7.0	5.2	2.9	2.4	6.6	8.8
p73+/-	1 / 53	4 / 125	10 / 54	24 / 47	19 / 76	2 / 47	0 / 135	15 / 50	40 / 51
	4 / 102	5 / 134	10 / 67	11 / 27	14 / 60	0 / 75	0 / 120	17 / 90	29 / 37
	0 / 97	3 / 98	14 / 50	16 / 54	15 / 59	4 / 143	0 / 114	18 / 92	29 / 35
	0 / 71	3 / 142	14 / 41	22 / 64	18 / 66	2 / 126	9 / 142	12 / 57	20 / 33
	4 / 78	2 / 189	12 / 65	12 / 29	18 / 62	0 / 110	5 / 117	23 / 97	19 / 24
	0 / 70	2 / 74	9 / 48	34 / 72	10 / 44	1 / 54	0 / 124	13 / 61	28 / 36
	8 / 125	0 / 110	6 / 29	12 / 33	11 / 40	2 / 54	0 / 132	17 / 77	35 / 48
	5 / 73	7 / 114	12 / 66	10 / 34	13 / 58	1 / 42	0 / 129	15 / 72	55 / 87
	1 / 60	2 / 98	8 / 41	14 / 54	12 / 39	6 / 126	2 / 150	13 / 78	75 / 103
	1 / 53	5 / 130	5 / 50	14 / 37	18 / 52	1 / 21	0 / 142	15 / 54	75 / 109
	4 / 78	4 / 99	15 / 48	13 / 27	12 / 53	0 / 84	0 / 119	15 / 42	39 / 58
	3 / 59	8 / 145	12 / 61	9 / 25	11 / 45	2 / 42	4 / 121	15 / 62	28 / 40
	3 / 70	3 / 63	9 / 52	15 / 27	26 / 64	0 / 115	0 / 129	9 / 39	25 / 34
	1 / 80	7 / 102	13 / 54	14 / 40	16 / 50	3 / 38	7 / 135	17 / 66	40 / 50
	1 / 62	13 / 172	15 / 95	17 / 49	10 / 46	1 / 44	4 / 88	11 / 62	20 / 29
	0 / 97	8 / 92	16 / 77	24 / 54	11 / 43	1 / 46	3 / 98	15 / 78	28 / 38
	0 / 74	6 / 135	8 / 54	25 / 53	14 / 41	2 / 74	4 / 104	9 / 44	46 / 64
	4 / 64	5 / 150	31 / 143	16 / 31	10 / 36	1 / 62	8 / 151	11 / 70	39 / 55
	0 / 78	13 / 155	14 / 65	26 / 52	12 / 49	1 / 190	0 / 132	21 / 79	34 / 44
	1 / 60	5 / 82	15 / 78	20 / 34	16 / 53	3 / 126	0 / 75	12 / 88	35 / 47
	4 / 84	7 / 117	15 / 72	35 / 55	15 / 72	1 / 48	0 / 94	18 / 84	35 / 48
	0 / 96	1 / 87	32 / 121	46 / 64	20 / 78	2 / 60	0 / 124	19 / 87	40 / 55
	1 / 65	4 / 94	16 / 76	32 / 47	10 / 54	2 / 252	0 / 68	18 / 73	38 / 56
	1 / 68	5 / 75	12 / 61	25 / 43	10 / 42	4 / 68	1 / 110	24 / 79	36 / 45
Average % Positive	2.5	4.4	20.6	45.7	26.7	2.6	1.6	22.6	73.2
Standard Deviation	2.4	2.3	5.3	12.5	5.1	2.0	2.2	5.0	5.5
p73-/-	2 / 40	17 / 180	4 / 88	16 / 28	8 / 38	4 / 54	4 / 55	1 / 55	30 / 36
	3 / 106	13 / 140	3 / 66	22 / 32	7 / 36	3 / 56	11 / 38	0 / 54	21 / 26
	3 / 56	8 / 98	2 / 64	13 / 28	9 / 45	6 / 108	10 / 50	2 / 25	25 / 32
	1 / 63	6 / 146	2 / 40	20 / 37	11 / 53	1 / 92	9 / 104	1 / 54	47 / 58
	2 / 38	18 / 165	2 / 54	20 / 38	19 / 90	3 / 79	5 / 44	0 / 54	35 / 43
	4 / 50	13 / 110	2 / 50	19 / 31	16 / 73	0 / 63	13 / 32	0 / 27	23 / 28
	6 / 68	3 / 66	2 / 48	22 / 30	11 / 59	2 / 79	3 / 38	2 / 41	33 / 42
	1 / 75	7 / 106	2 / 40	28 / 43	12 / 55	0 / 55	2 / 45	3 / 52	45 / 53
	1 / 42	18 / 155	3 / 55	38 / 59	14 / 69	4 / 71	7 / 40	2 / 50	21 / 25
	2 / 57	14 / 170	2 / 39	28 / 44	15 / 72	1 / 61	4 / 30	2 / 51	41 / 56
	2 / 77	8 / 70	0 / 36	36 / 56	8 / 41	3 / 96	4 / 48	2 / 30	32 / 45
	4 / 60	9 / 120	0 / 62	30 / 46	10 / 45	1 / 69	4 / 34	4 / 65	43 / 51
	3 / 54	20 / 190	0 / 56	16 / 28	15 / 70	4 / 107	6 / 41	2 / 40	49 / 62
	0 / 62	6 / 71	0 / 74	18 / 24	10 / 82	4 / 65	2 / 50	2 / 79	36 / 40
	2 / 84	8 / 79	4 / 55	27 / 31	9 / 45	1 / 96	5 / 45	2 / 40	27 / 34
	2 / 67	5 / 54	0 / 54	37 / 51	13 / 73	0 / 63	5 / 51	0 / 22	33 / 40
	3 / 80	3 / 49	2 / 24	18 / 25	9 / 41	5 / 68	8 / 63	0 / 45	40 / 48
	0 / 68	19 / 147	3 / 54	7 / 11	5 / 55	5 / 92	9 / 54	1 / 49	21 / 25
	3 / 65	7 / 63	1 / 27	25 / 33	8 / 51	0 / 54	9 / 71	2 / 47	28 / 35
	4 / 103	11 / 116	3 / 50	17 / 21	9 / 60	1 / 78	6 / 40	0 / 50	33 / 40
	2 / 53	3 / 118	2 / 41	27 / 41	14 / 72	3 / 87	2 / 28	1 / 41	28 / 35
	3 / 68	2 / 101	3 / 51	17 / 28	6 / 29	4 / 70	3 / 74	1 / 66	36 / 41
	2 / 63	4 / 115	3 / 65	19 / 35	9 / 48	5 / 104	3 / 62	0 / 44	17 / 21
	1 / 74	8 / 89	3 / 40	25 / 42	7 / 42	2 / 78	2 / 82	1 / 40	27 / 31
Average % Positive	3.7	8.3	4.1	65.0	19.0	3.3	12.3	2.8	81.6
Standard Deviation	2.2	3.1	2.5	9.5	3.2	2.5	8.5	2.5	4.2
p63-/-	10 / 92	18 / 87	67 / 115	24 / 149	1 / 51	1 / 53	0 / 48	32 / 61	40 / 92
	5 / 48	28 / 196	79 / 123	37 / 171	0 / 49	7 / 75	0 / 75	45 / 78	48 / 117
	4 / 52	9 / 99	76 / 128	17 / 141	2 / 44	3 / 39	0 / 44	36 / 64	47 / 94
	10 / 65	10 / 71	73 / 127	13 / 140	0 / 56	4 / 102	0 / 42	29 / 61	47 / 112
	6 / 91	16 / 67	95 / 170	19 / 136	0 / 62	2 / 65	0 / 51	49 / 93	59 / 141
	5 / 50	8 / 48	73 / 121	23 / 145	0 / 68	3 / 71	0 / 39	39 / 94	45 / 92
	8 / 100	8 / 65	43 / 89	14 / 94	2 / 53	4 / 78	0 / 33	38 / 75	45 / 108
	7 / 95	13 / 134	55 / 98	13 / 53	3 / 58	1 / 75	0 / 67	39 / 69	44 / 97
	5 / 91	13 / 120	67 / 96	9 / 97	1 / 52	1 / 42	0 / 49	49 / 83	55 / 116
	3 / 40	25 / 80	44 / 79	8 / 63	0 / 72	2 / 57	0 / 47	68 / 101	30 / 72
	6 / 54	24 / 139	117 / 191	8 / 74	1 / 29	2 / 77	0 / 52	40 / 68	45 / 105
	6 / 75	12 / 80	90 / 153	11 / 121	0 / 60	4 / 60	0 / 84	43 / 96	52 / 123
	12 / 130	11 / 74	35 / 63	18 / 107	2 / 48	3 / 45	0 / 56	79 / 152	35 / 73
	12 / 96	16 / 109	61 / 97	22 / 145	1 / 62	5 / 66	0 / 62	36 / 83	35 / 91
	16 / 114	13 / 91	48 / 94	4 / 48	1 / 63	2 / 84	0 / 133	32 / 76	57 / 123
	5 / 51	6 / 73	34 / 64	4 / 44	0 / 48	3 / 67	0 / 59	28 / 69	83 / 140
	7 / 70	17 / 130	56 / 94	6 / 59	1 / 60	4 / 80	0 / 117	29 / 60	45 / 90
	5 / 65	6 / 69	55 / 87	11 / 63	0 / 64	0 / 76	0 / 84	39 / 74	50 / 103
	4 / 63	18 / 103	32 / 49	8 / 88	0 / 42	3 / 65	0 / 76	29 / 50	28 / 62
	4 / 50	9 / 79	57 / 83	6 / 44	1 / 48	4 / 78	0 / 47	55 / 127	25 / 55
	7 / 65	8 / 57	72 / 99	5 / 54	2 / 54	2 / 53	0 / 80	68 / 134	50 / 102
	6 / 68	13 / 149	78 / 104	7 / 56	0 / 61	5 / 68	0 / 53	33 / 80	28 / 64
	2 / 50	14 / 66	78 / 112	37 / 209	1 / 77	5 / 63	0 / 76	43 / 93	62 / 148
	6 / 51	25 / 180	50 / 88	20 / 147	0 / 66	1 / 75	0 / 65	45 / 104	35 / 88
Average % Positive	9.2	14.8	60.8	13.5	1.5	4.5	0.0	50.3	45.2
Standard Deviation	2.7	5.4	6.8	4.2	1.7	2.4	0.0	7.1	4.5

Table S4. Cilia-Associated Gene Set

MGI Gene Symbol									
Ncs1	Nek2	Slc1a4	1700019L03Rik	Dnaic1	Mthfd2l	Trip13	Pddc1	B4galt5	Atp13a2	Kif24
Ccdc67	Elmod1	Cntrob	1700026D08Rik	Dnaic2	Mtr	Trnp1	Cyp2s1	Ephx4	Ehf	Api5
1700007G11Rik	Zfyve19	Rbmx2	1700028P14Rik	Dnd1	Mtss1l	Troap	Dgcr6	Ccnj	Blzf1	Psmd10
Foxj1	Ccdc30	Nphp1	1700066M21Rik	Dpy19l2	Muc5b	Trp73	3110082I17Rik	Lpar6	Ect2	Pfdn2
1110017D15Rik	Fignl1	Slc38a1	1700084C01Rik	Dpysl5	Myo5a	Ttc12	Adi1	Ankib1	Kctd4	Rfx3
Stk33	Sptlc3	Nln	4930427A07Rik	Dydc2	Nags	Ttc16	Gm3500	Pmf1	Rbm19	Ercc3
Spag17	Mns1	Tmem107	4930503B20Rik	Ecscr	Naip1	Ttc22	Fgfr1op	Pak3	Zfp692	Gale
Ccdc39	Vwa3a	Ublcp1	4931429I11Rik	Efhb	Neto2	Ttc29	Fam193b	Ddx39	Ipo7	Btf3l4
Lrriq1	Lrguk	Plch1	4932438H23Rik	Efna2	Neurl1a	Ttc30a2	Nsg1	Upk2	Zfyve9	Ccnc
Efhc1	Naa40	Sdccag8	4933427G17Rik	Eml1	Nr5a2	Ttk	Rhou	Tmem184c	Tex9	Taf9b
Lrrc23	Top2a	Spag6	9230112D13Rik	Ephb2	Nrip3	Tubg2	Htr2b	H1fx	Tmem69	Mkl2
Mlf1	6430531B16Rik	Phc1	AA467197	Erp27	Ntsr2	Ubash3a	Tfdp1	Bbs2	Cenpj	Ttf1
6820408C15Rik	Frrs1	Fam118a	Aard	Exo1	Nudt12	Ubxn10	Cntd1	Plk4	St14	Dpcd
Traf3ip1	Zfp354b	Lig1	Acsm1	Fam109b	Oip5	Ugt8a	Alkbh2	Il12rb2	Aldh3a2	Ift52
Kif9	2610028H24Rik	Scrib	Actl7b	Fam132b	Oit1	Uhmk1	Vill	Ercc6l	Ccdc122	Zfp791
Lrrc36	Asrgl1	Tsr1	Agr3	Fam149a	Olfr19	Unc5c	Fbxo30	Cmas	Krr1	Lnx1
Fank1	Riiad1	Prodh	Agtr1a	Fam179a	Olfr798	Vash2	Khdrbs3	Zfyve1	Fkbp4	Fhdc1
Enkur	Tm4sf1	Haus4	Ak8	Fam19a5	Osbpl3	Vit	Gpx2	B230118H07Rik	Sorbs1	B3galt2
Tekt4	Fam188b	Gm20604	Amn	Fbxo21	Palb2	Wdr38	Ccdc138	Cbx7	Bmp2	Lypla2
Ccdc40	1700012B09Rik	Myb	Ankrd42	Fgl1	Pappa2	Wdr73	Pnck	Utp15	Acbd7	Ppil6
Hs6st2	Fam81a	Fbxo36	Aox1	Flywch1	Pbk	Xk	Kif3b	Zfp821	Kif3a	Orai3
Ccdc113	Wdr63	Rangrf	Apobr	Fmn2	Pgbd5	Xlr4b	Fam118b	Supv3l1	Rpf2	Sharpin
Wdpcp	Efcab1	Poli	Armcx6	Fxyd1	Pklr	Zcchc4	Gmcl1	Mnt	Arhgap24	E2f5
1700016K19Rik	Adam15	Coro2a	Asb17	Galnt6	Poteg	Zfp474	Ccdc51	Tfap4	Eif6	Gnpnat1
Nek10	Dnajc28	Rab3ip	Aspm	Gemin6	Prdm8	Zfp770	Tulp3	Ripk2	2310007B03Rik	Tm7sf3
Cdk1	Ak7	Pno1	Atp10b	Ghrl	Prkar1b	Zscan12	Dpagt1	Smarcad1	Rnf170	Akt2
Mdm1	Wdr34	4833427G06Rik	Atp13a5	Gja6	Prkg2	Rad23a	Ccdc78	Wrap53	Ptgr2	Ctnnbl1
BC051019	Mak	Zfp54	BC048403	Glb1l2	Prr19	Rps6ka5	Alg11	Taf11	Znhit1	Ercc6
Nme5	Cdc25c	Ttc25	BC049715	Glipr1	Prss48	Gm5796	Zbed4	Alms1	Mta1	Phf6
Rsph1	Smarcd2	Lmln	Bcl2l10	Glis3	Pyroxd2	Tsen15	Zfp330	Erbb2	Npm3	Bmp8a
Sorbs2	BC055324	Ankrd32	Bcl2l14	Glra3	Rac2	Rsph3b	Agpat9	Rab36	Mblac1	Arl3
Melk	Foxn4	Fsip1	Bok	Glrp1	Rad51ap1	Morn5	Ap4b1	Cep192	Ppp1r36	Cul7
Calb2	Rnf32	Odf3b	Bub1b	Glt1d1	Rad54b	Pde9a	Eepd1	Dzip1l	G6pc3	Dtwd2
Mcm8	Ulk4	Chek2	Bysl	Gm10267	Rd3	AW554918	Kpna1	Klhl21	Itga7	Fyco1
Ckap2l	Rsph9	Kcnip4	C1ra	Gm11487	Rel	Ndc80	Prdm15	Cep57l1	Ccdc132	Commd9
Fam161a	Tnn	Dcdc2a	C8g	Gm1661	Rgs4	Hspa1l	Wdr76	Osgepl1	Hsd17b14	Cks2
Ccno	Gins2	Bin3	Calcoco2	Gm3139	Rhobtb2	Rbp4	Cpeb2	Edc4	Spef1	Ebp
Efcab10	1700003M02Rik	Cep164	Capn6	Gm3286	Rhpn1	Haus5	Bola1	Gm3696	Cdc27	Bphl
Dnajb13	Itih2	Oraov1	Caps2	Gm3448	Ribc1	Akr7a5	Zfhx2	Zfp51	Cbx2	Uchl5
Lrwd1	Chmp6	Spa17	Car10	Gm428	Rinl	Asap2	H2-Q10	Gprc5c	AI314180	Inpp5f
2010107G23Rik	Ccdc60	Pacrg	Casc1	Gstcd	Scgn	Tmem138	A430033K04Rik	Slu7	Tdp1	Brd8
Kndc1	Ankrd54	Gm166	Casc5	Gtf2a1l	Scml2	Gm2897	Trnt1	1600002K03Rik	Tep1	Aurka
Spata24	1700026L06Rik	3830408C21Rik	Ccdc103	H1fnt	Scn3b	Flnb	Tmem231	Lin9	Crim1	Sox2
Nek5	Agbl2	Nudc	Ccdc153	H2-T22	Scrn3	Chn1	9130023H24Rik	Dhx30	Prr14	Cyb561d2
1700029J07Rik	Ttll13	Wdr90	Ccdc158	Hcn2	Sfrp1	Gpr85	Sae1	Rnf123	Pcm1	Fmod
Dnali1	Cdc20	Atr	Ccdc24	Hdac8	Sh3bp1	Tnfrsf1b	Iqsec2	Ttc8	Bbs1	Fastkd2
Fhad1	Akap14	Flrt1	Ccdc42b	Hirip3	Sidt1	Rgs3	Ogg1	Actr6	Cspp1	Poc5
Lrrc51	Znrf2	Anxa8	Ccdc65	Hpgd	Slc10a2	Rsl24d1	Tmem144	Calml4	Ddit3	Lpar4
Pde3b	Omd	Dixdc1	Ccdc74a	Hrasls	Slc10a5	1110004E09Rik	Cd83	Rabl2	Dgke	Odf2l
Fam183b	Cmpk2	Dynlrb2	Ccdc89	Hspb6	Slc35e4	Tmem194	Dock8	Cetn2	Lrrfip2	Atg16l1
Fbxo16	Cby1	Heatr5a	Ccl20	Hspb9	Slc38a3	Ndufaf3	Mrpl39	Slc25a19	Syt11	Otud6b
Zmynd10	Dync2h1	Lypd6b	Ccnb1	Hyls1	Slc38a6	Tyro3	Gas2l3	Nfkb1	Fkbpl	Slc25a17
Tekt1	Lrrc48	Isyna1	Cd177	Iglon5	Slc47a2	Katnal1	Zfp41	Impad1	Lonp2	Ppp6c
Gm10639	Tsnaxip1	Sclt1	Cd27	Il27	Spag16	2610301B20Rik	Psmg2	Tex10	Noxa1	Kremen1
Gsta2	Capsl	Cc2d2a	Cdca5	Inca1	Spag5	Daglb	Oscp1	Zfp341	1700123O20Rik	Ccnb2
Olfml2b	Cdkl4	Cep152	Cdk20	Iqcd	Spag8	Afap1	Angptl7	Arc	Ascc1	AK010878
Agr2	Smc2	Gpn2	Cenpa	Itgae	Spata18	Ap3m2	1700007K13Rik	Stxbp4	Tubb4b	Arl6ip6
Zfp667	9230110C19Rik	Sgk3	Cenpe	Itgam	Spata20	Slc12a4	Copg2	Pcsk6	Glt8d1	Hsdl1
Lrrc46	BC022687	Ahsa1	Cenph	Itgb4	Spc25	H2afx	Pygm	Bmp8b	Alg5	Dtymk
Cacnb3	Gmfg	Trp53inp1	Cenpk	Jsrp1	Spsb4	Cox6b2	Six1	Me2	Eif5b	Gabrp
Fermt1	L3mbtl2	Abhd14a	Cenpp	Kcnk7	Srgn	Ttn	Prc1	Eif2ak2	Inpp1	Zfp59
Ttll6	Iqca	Efcab2	Cenpv	Kif2c	Stard5	Acvr1b	Wdr35	2610015P09Rik	Adck3	Mum1
Spef2	Myh10	1110008L16Rik	Cep55	Kif6	Stk32a	Tppp3	Ciapin1	Rhbdd3	Six4	Nhsl1
Stil	Dtl	Cklf	Cep97	Kntc1	Syt17	Tcea2	Kif1a	Dhx29	Amacr	Pygo2
Usp2	Ypel1	Gm15800	Ces1b	Lace1	Sytl1	Cenpf	Nprl3	Lgals12	Hectd3	Cep63
Efhd1	Meig1	Oxa1l	Ces1c	Lce1a1	Tacc3	Gpd1	Man2c1	Eefsec	Ttc30b	Emp3
Ccna1	Tal2	Hspa4l	Chga	Lfng	Tbc1d22b	Spg21	Pdxk	Pbx4	Tagap	Strbp
Bcas1	Tmem29	Jag1	Chrm1	Lrrc17	Tbcc	Cars	Cryaa	Arid4a	Napg	Pram1
Lca5	Wdr78	Ccdc151	Chst11	Lrrc18	Tcte3	Hist1h2ae	Ube2t	Ccdc61	Tagap1	Tsga10
Ropn1l	Ccdc108	Ift74	Cmbl	Lrrc43	Tctn3	Rars	Eri1	Rcbtb2	Txndc12	B9d2
Fbp1	Serac1	Aldh3b1	Cox10	Lrrc56	Tekt2	Kctd12	Slc22a21	Pxk	Ift88	Gm9833
Qsox1	Mast2	Ccdc146	Crispld2	Lrrc6	Tha1	Foxo1	Qser1	Kif20a	Hipk1	Edar
Armc4	Gm7173	Sord	Csf3r	Lrrc9	Thrb	Fbxl4	Trp53	Terf1	Maged2	Casp6
Tbx1	Iqub	Mycbp	Cxcl12	Ltbp2	Tiam1	Rrm1	Zfp329	Ruvbl2	Haghl	Mfap1b
Egln3	Nek4	Bicd1	D1Ertd622e	Mcm3	Tmem102	Rsph3a	Atp6v1h	Arhgap11a	Zfp362	Noc4l
Gsta1	Sass6	Ets1	D330045A20Rik	Mcph1	Tmem104	F2rl1	Spice1	Gbf1	Orc3	Psmb8
Zfp382	Ccdc17	Pex3	Dapl1	Mdh1b	Tmem38a	Pgap3	Stx16	Uap1	Meaf6	1110032A03Rik
Spata17	Tmem201	Parn	Dcdc2b	Med12l	Tmem52	Spata2	Rpgr	Rasgrf1	Aasdhppt	D430042O09Rik

Lrrc34	Fam161b	Pom121	Dhx58	Mfsd12	Tmprss9	Dsel	Pdgfrl	Phrf1	Cep57	Cenpw
1700001C02Rik	Ccdc114	Morn2	Dlec1	Mks1	Tnip1	Hace1	Odf2	Dyx1c1	Hpx	Ino80c
Gm11992	Pih1d2	1700001L19Rik	Dlgap5	Morn4	Tnnt1	B9d1	Gzmm	Lrpprc	Ttc21a	Alkbh3
Ubxn11	Ralgps2	1700011H14Rik	Dll4	Mpp4	Tomm20l	Clec11a	Ovol1	Zdhhc24	Ermp1	Gm14326
4930444P10Rik	Cep170	1700019D03Rik	Dlx4	Mrs2	Trib2	Irak1bp1	Trit1	Cks1b	Prrg4	Vps33b
Dnaja3	Banp	Sgcb	2700049A03Rik	Sgpp1	Pcdhgb4	Zfp655	Uqcrc1	Wdr48	Acrbp	Gtf2h2
Oma1	Pemt	Strada	Nr2f2	Ehmt2	Rad1	Naa35	4930404N11Rik	Rnf26	Tigd2	Lrp1
Bcorl1	Tcp11	9530077C05Rik	Faf2	Gm684	Zfp609	Pole3	Dusp8	Junb	Ankrd17	Isoc1
2700094K13Rik	Eif3d	Nek1	Nedd1	Xlr3c	Phtf1	Arl6	Rrp15	B4galt3	Gjb4	Nme7
Pard6g	Cd14	Hmgb2	Mrps7	Herpud2	Gpr137	Mios	Mtg1	Trim23	Snap47	Gltscr1
Prkcsh	1700003E16Rik	Iqck	Atp6v0d1	Pgam5	Chchd7	Ift46	Rmnd5b	Lrrc49	Sqle	Golga3
Cd320	U2af2	Erlin2	Cul4b	Brf1	Bzw1	Pisd	Atp5s	Grhpr	Dtnbp1	Zfp607
Mipep	Ccdc85b	Ppp2r3d	Ccrn4l	Mllt10	Lpcat4	Ipo9	Fam160a2	Fbxo32	Adam17	Cherp
Slmo2	Crnkl1	Zfp771	Csrp2	Anapc4	Rbm7	2610528J11Rik	Zfp943	Zfp367	Entpd7	Ppp4r2
Commd5	Fzd3	Dnlz	Cd55	Pik3c2b	1700093K21Rik	Mre11a	Hist2h2bb	Tmem57	Idh3g	Ankrd10
Yif1b	Ep400	Txnl4a	Sap25	Hibch	Trap1	Bcl2l12	Shmt1	Hist1h2an	Tuba1b	Rad21
Ccdc34	Arl4a	Rangap1	Slc35a4	Aarsd1	Amfr	Adsl	Dis3l2	Lztfl1	Usp28	Tbl3
Dnajc7	Pla2g16	Tuba1a	Rbm34	Churc1	Cct8	Pfn2	Rdh10	Josd2	Tmem38b	Pop4
Bccip	Ap3b1	Mrps17	Cdca2	Tjap1	Nus1	Zrsr2	Mum1l1	Rufy1	Wdr61	Mboat7
Pqlc3	Mrpl49	Ccdc88c	Chchd6	Tmed5	Gapvd1	Pola1	Hspa2	Mphosph9	Ctxn1	Fancl
Plekha7	Wdr92	Xpc	AI597479	Sccpdh	Pepd	Ccdc18	3010026O09Rik	Cited1	Ddx23	Ctnnd1
Ranbp1	Taf9	Lxn	Gtpbp4	Ap2b1	Fyttd1	BC023829	Wdr60	2310030G06Rik	Iqgap2	Tfpt
Uevld	Lpar3	Aifm2	1190007I07Rik	Thada	Aagab	Gstm4	Ooep	Ttll5	Bub3	Dhx9
Fahd2a	Drg1	Rsbn1l	Dhx40	Vrk1	Rc3h2	Alkbh6	Dpy30	Bms1	Irak2	Ttbk2
Tfb2m	Zfp422	Atic	Pycard	Dtx3	Lsm6	Abcf2	Pim2	Acyp1	Polr2d	Ddx3y
Elof1	Upf3b	Yeats2	Piga	Raph1	Ncoa2	Gnl1	Stx17	Mfsd10	Mef2d	Idh3a
Cep350	Fam60a	Nin	Btc	Pms2	Chrac1	Psip1	Zdhhc4	Lsm3	Psmf1	Echs1
Scap	Pcdh10	Ppil2	Fzd7	Mcm7	Creld2	Tec	Odc1	Smad3	Cinp	Psmc3
Prps1	Stxbp2	Med24	Ift20	Hist1h2ai	Pop1	1700088E04Rik	Tspan31	Zfp961	Lin7c	1110004F10Rik
Kctd3	Ciao1	Nmnat1	Abcf1	Ddx50	Epha1	Dap3	Fiz1	Polr3b	Pgbd1	Fkbp14
Nmt1	Uhrf1	Rabggtb	Sgsm3	Immp2l	Tmem218	Impa1	Btrc	Tex2	Mlh3	Fgfr3
Med31	Sod2	Hist1h2af	Dph3	Xpnpep1	Ubxn4	Nlgn2	Ecsit	Pebp1	Appl1	Tnrc6b
Eps8	Zdhhc2	Pfkl	Akr1b8	Ilf2	Med28	Nfatc2ip	Sec11c	Nsdhl	Eftud1	Cct4
Id4	Carhsp1	Ndufa9	Mphosph10	Rbpj	Wdr77	Thoc3	Cd3eap	B230219D22Rik	Sox11	Nf2
Als2	Wrb	Tubg1	Psmd3	Klhl15	Nhp2	Uba3	Ttll4	Crybg3	Zmat3	Ecd
Kbtbd3	Uba7	Smu1	Olfr543	Mrpl10	Rnf7	Ddt	Bri3bp	Ston2	Prdm4	Nsmaf
Fam126b	Mif4gd	Upf1	Kdsr	Flii	Fxn	Scoc	Gfm1	Zhx1	Maz	Rpgrip1l
Mrpl24	2010012O05Rik	Rbl2	Bik	Uck1	Atp6v1c1	Tmem53	Mesdc2	Slc35b1	Mapk7	Mettl15
Exosc9	Ssbp3	Hsp90aa1	Sirt3	Sec31a	Psmd9	Dopey1	Rasa4	Mbd1	Tfg	Ccdc117
Slc1a3	Itpka	Gtf3c5	Pdhb	Gtpbp10	Trak1	Srpk1	Frmd4b	Rae1	Ppp2r3a	Bpnt1
Slc35e2	Tmem101	Cdyl	Ildr2	Rsrc1	Pkig	Megf6	Pkd2	Anapc10	Smpd1	Nde1
Acot7	Poc1a	Ppa1	Tmem181a	Rassf6	Sh3gl1	Ttc17	Hist1h2ag	Hmga1-rs1	Hnrnph2	Pbx1
Txndc11	Sdr42e1	Mkks	Fsd1l	Pttg1	Tmem50b	Klhdc3	Dap	1110051M20Rik	Lrrcc1	Ppfia1
Zfp444	Ftsj2	Rbm6	Ssna1	1700001P01Rik	Zfp954	Tmtc4	Nup88	Parp1	Morn1	Eif2b2
Entpd5	Fbxo18	C87436	Ptges3	Sec24b	Zc3h6	Ppid	Abi2	Ugt1a6a	Asf1b	Wdr70
Hspa4	Wdr47	Rab43	Adprh	Sdcbp	Cops6	Eif4enif1	Zbtb44	Slc25a10	Spata13	Cxxc1
Rpap3	Psmd6	Ralgds	Ddr1	Timm13	Gm14306	Tnpo3	4921506M07Rik	Adrm1	Pcyox1	Far2
Gsto2	Zbtb38	Med18	Pcnt	Vamp4	Cep135	Fbxl14	Hist1h2ah	Pmpcb	Uty	3110062M04Rik
	Slc35a5	Dmkn	Mbnl3	Mob3b	Hnrnpul1	Gripap1	Gstm1	Hprt	Srrt	Abhd10
	Aftph	Dcun1d2								

Supplemental Figure Legends

Figure S1. Generation of the p73$^{floxE7-9/}$ Mice, Related to Figure 1 (A) Schematic representation of the targeting strategy used to conditionally delete exons 7, 8, and 9 of p73. Red triangles denote the introduced loxP sites. Black circles represent Frt sites utilized to remove the neomycin resistance cassette (NeoR) (orange box) by crossing with a FlpE deleter mouse (Rodriguez et al., 2000). The red rectangle marks the location of an exon 14 Southern probe for identification of recombinant clones in combination with Cla1 and HindII restriction enzymes. A second probe located outside the long DNA homology arm that was used to screen the mESCs. Clone 2A7 (**) had germline transmission leading to the mice utilized for this study. (B) Sanger sequencing of a PCR product from lung cDNA indicates in-frame splicing of exons 6 and 7 (p73+/+) and exons 6 and 10 (p73-/-). (C) qRT-PCR of lung cDNA was performed using primers within exon 5, across the exon 6/7 boundary, and within exon 10 of p73. Data are represented as normalized ratios of p73-/- to p73+/+ mRNA expression. (D) Western analysis of protein harvested from lung tissue of the indicated genotyped animals shows absence of full-length p73 protein in the p73-/- animals and a faster migrating immuno-reactive band in the p73+/- and -/- samples, with a molecular weight consistent with expression of a p73 protein lacking exons 7-9 (* = non-specific band). (E) Micrographs of MTECs isolated from tracheas of p73+/+ or p73-/- animals, infected with non-silencing (NS) or two different p73 short hairpin RNA silencing constructs (shRNA 1 & 2), and grown in

differentiation media. Representative IF staining of p73 (red) and *α-tubulin (green) is shown for each condition. Arrows indicate cilia and flagella within p73+/+ animals.

Figure S2. p73-/- Mice Show Evidence of Infection and Inflammation in the Lung, Sinus and Ears, Related to Figure 2 (A) Representative images of alcian blue (top panel) and H&E (bottom panel)-stained lungs from p73+/+ and p73-/- mice. Mucin-producing cells and retained mucus are stained blue. (B) Representative H&E images of sinus and ears of p73+/+ and p73-/- mice. The external ear canal (EC), middle ear (ME), tympanic membrane (TM) and malleus (M) are labeled. Arrows indicate areas of mucus and inflammation in the upper and lower panel, respectively.

Figure S3. Representative Images from the Trachea and Bronchioles Used for the Quantification of Respiratory Epithelium Cell Types Shown in Figure 3, Related to Figure 3 as well as Table S1 IF detection of the indicated proteins in murine tracheal and bronchiolar tissue from mice of the indicated genotype. Foxj1 (green) was used as a marker of the ciliated cells. Scgb1a1 (red) was used as a marker of club cells. Alcian blue staining was used to detect mucin-producing goblet cells. Pgp9.5 (yellow) was used as a marker of neuroendocrine cells. p63 (red) was used as a marker of the basal cells within the murine trachea (scale bars = 25 μm).

Figure S4. p73 is Expressed in Ciliated and Basal Cells Within the Human Airway, Related to Figure 4 Representative IF micrographs for the indicated proteins on sections of lung tissue from ten individual human patients . (A) *α-tubulin (green) and p73 (red) staining is consistent with a much higher percentage of MCC in human bronchiolar epithelium as compared to murine. (B) Foxj1 (green) and p73 (red) staining showing basal cells with single p73 positivity as well as luminal MCCs with co-expression of p73 and Foxj1. (C) p63 (green) and p73 (red) IF shows basal localization of p63 while p73 protein expression patterns are similar to that observed in the murine tracheal epithelium - both basal and ciliated (scale bar= 50 μm).

Figure S5. Analysis of DNA-Binding Profiles after *in situ* Protein-DNA Crosslinking and ChIP-seq (p73, p63 and Pol II) of Murine Tracheal Cells Related to Figure 5 and Table S2 (A) Heatmap of hierarchically clustered Pearson correlations between ChIP-seq samples. (B) Analysis of the genomic features of the p73, p63 and Pol II binding sites. The first column under each protein section indicates the number of peaks observed within each respective genomic feature. The second column indicates the log ratio of binding enrichment for the peaks identified over the expected overlap based on the size of the given genomic feature. The final column lists the p-values for the observed enrichment of each feature type. (C) Summary of the number of binding sites and median

distance to transcriptional start sites (TSS) for the Pol II, p73, and p63 ChIP-seq datasets. (D) CDF plot comparing the RNA expression levels of genes bound by p73 within 25,000 kb of their TSS versus genes not bound. Significance testing was performed using the Kolmogorov-Smirnov test. (E) Binding motifs identified in p73 and p63 ChIP-seq peaks. (F) Table of binding profiles of known target genes Mdm2 and Cdkn1a, including the q-value significance of the binding sites observed at each of the genes, and the bp distance from the middle of each binding site to the TSS, along with notation for whether a corresponding p63 binding site was found at the same location. Below the table are Integrative Genomics Viewer screenshots of Mdm2 and Cdkn1a in which the four tracks show ChIP-seq data normalized to 1x depth of coverage and presented with identical scales. The bottom three tracks represent DNA reads that were obtained following ChIP with the antibodies listed to the left, and the top track is the input sample for comparison. At the bottom of each panel is an annotated exon/intron gene structure displayed on the same scale as the ChIP-seq tracks with a gray arrow at the bottom annotating the gene orientation.

Figure S6. Additional p73 Binding to Novel Target Genes in Cilia-Associated Gene Set, Related to Figure 5, Table S2, Table S3, Table S4 and Table S5 At top, a Venn diagram illustrates the overlap of genes featuring a p73 binding site within 25 kb of their transcriptional start site (930 total) with the cilia-associated gene set (1398 total) (Treutlein et al., 2014). The 105 overlapping

genes are detailed at bottom. For each gene, the q-value significance and distance to the respective TSS for the associated binding sites are indicated along with notation for whether a corresponding p63 binding site was found at the same location. Genes are ranked by decreasing q-value and are highlighted in gray if they were significantly differentially expressed after exogenous overexpression of p73 in either p73+/+ or p73-/- MTEC cultures, as described in Figure 5.

Table S1. Quantification of Epithelial Cells within Pulmonary Epithelium, **Related to Figure 3.** Table of 24 fields of view analyzed to determine percentage of positive cells as presented in Figure 3, with representative images present in Figure 3S. The data are represented as number of positive cells over the total number of nuclei present within 0.02 mm^2 for IF micrographs (neuroendocrine, basal, club, and MCC) and 0.15 μm^2 for micrographs of alcian blue staining (mucin). Data are represented for each genotype and grouped for each of the cell types that make up the tracheal and bronchiole epithelium. Also included are the "average percent positive" cells with standard deviation for an indicated epithelial cell type of a given genotype relative to all epithelial cells within the area for 24 fields counted.

Table S2. Complete List of Genomic Binding Sites Identified Through ChIP-seq for p73, p63 and Pol II, Related to Figures 5, S5 and S6. Coordinates of

MACS2-identified genomic binding sites and Homer peak annotations for p73, p63, and Pol II are listed on individual sheets. For each ChIP-seq sample, peaks were annotated with the nearest GENCODE M7 TSS and protein coding TSS.

Table S3. RNA-seq Expression Profile of Murine Tracheal Epithelium, Related to Figures 5 and S5. TPM gene expression estimates are listed for all GENCODE M7 genes in the duplicate scraped tracheal epithelial RNA samples from p73+/+ animals.

Table S4. Cilia-Associated Gene Set, Related to Figures 5 and S6. Genes that have been published as MCC cell type marker genes and were used in our analysis (Treutlein et al.,2014). Genes unique to MCCs and only those genes matching to Gencode M7 protein coding genes and standard chromosome locations are listed for reference.

Table S5. RNA-seq Expression Profile of p73+/+ and p73-/- MTECs After Ectopic p73 Expression, Related to Figures 5, S5 and S6. The raw read count table used as input for differential gene expression analysis. Expression was conducted in duplicate for each condition as indicated. TPM gene expression estimates are included as a separate sheet for reference.

Extended Experimental Procedures:

Protein harvest and immunoblotting

Whole mouse lungs were homogenized and lysed in RIPA buffer and immunoblot analysis was conducted as previously described (Westfall et al., 2003) for p73 (EP436Y; Abcam) using 50ug of tissue lysate.

Histology and immunofluorescence

Mouse tissues were fixed in 10% neutral buffered formalin and paraffin embedded for sectioning. Alcian blue (pH 2.5) staining for mucin cells was performed as previously described (Hayat, 1993). Immunofluorescence was conducted using antibodies against Foxj1 (2A5; eBioscience), p63 (H129; Santa Cruz), p73 (EP436Y; Abcam), Pgp9.5 (ab8189; Abcam), Scgb1a1 (ab40873; Abcam), *α-tubulin (611B-1; Sigma), γ-tubulin (T5326; Sigma), Krt5 (20R-CP003; Fitzgerald), and Krt14 (20R-CP002; Fitzgerald). Amplification by TSA Plus Fluorescein System or TSA Plus Cyanine 3 System (Perkin Elmer) was used for detection of Foxj1, p63, p73, Pgp9.5, Scgb1a1, and γ-tubulin. *α-tubulin, Krt5, and Krt14 were detected using Alexa Fluor (Life Technologies) secondary antibodies. SlowFade Gold Antifade Mountant with DAPI (S36939; Invitrogen) was used as a nuclear marker. Immunohistochemistry was conducted using pan-cytokeratin (bs-1712R; Bioss) and anti-alpha smooth muscle actin (ab32575; Abcam) antibodies.

shRNA-mediated gene knockdown

shRNAs directed to the 3' untranslated region (shRNA 1-GAACTGCCCTTAGCTACATAT) and exon 6 (shRNA 2-AGTGTGGTTGTGCCGTATG) of p73 were purchased from Sigma Aldrich. MISSION TRC2 Non-Mammalian shRNA (Sigma Aldrich) was used as a negative control. Viral production and transduction was performed as previously described (Rubinson et al., 2003).

Scraped murine tracheal RNA harvest, qRT-PCR, and Sanger sequencing

RNA was harvested from tissue by scraping the epithelium of the trachea in Trizol and purified using the Aurum Total RNA Mini kit (Bio-Rad). qRT-PCR experiments were conducted using oligo(dT)-mediated first-strand synthesis and SYBR Green quantification. mRNA levels were quantified using primers targeting exon 5 (GACATGCCCCATCCAGATCA /AGCTCGTGGTTGGGGCAGCG), the exon 6/7 Junction (GTGGATGACCCTGTCACCGG/ GAAGTTGTACAGGATGGTGG) and exon 10 (GGTGACTCGGCCTCTGTAGG/ CTGGTCCTTCGAAATGACTAC) of p73. Sanger sequencing was conducted using identical primers.

Murine tracheal epithelial cell (MTEC) culture, exogenous expression, and RNA harvest

MTECs were isolated, cultured, and differentiated as previously described (Lam et al., 2011; Vladar and Brody, 2013). MTECs harvested from p73+/+ and p73-/- mice were infected twice (at time of plating and 12 h later) with TAp73β and Fg12-CMV control expression vectors as described previously (Rosenbluth

et al., 2011; Rosenbluth et al., 2008). For Fig. 6B, MTECs were grown as submerged cultures on collagen-coated plates for 3 d in MTEC growth media (DMEM/F12 supplemented with HEPES, L-glutamine, $NaHCO_{3,}$ penicillin-streptomycin, fungizone, insulin, transferrin, cholera toxin, EGF, bovine pituitary extract and FBS). For Fig. S1E and Fig. 6B, MTECs were grown as submerged cultures on collagen-coated plates for 3 d in DMEM and then switched to differentiation media containing 2% NuSerum for 3 d (Lam et al., 2011; Vladar and Brody, 2013). For Fig. 5 and Fig. S6, MTECs were grown in transwells containing MTEC growth media for 5 days and then lifted to air-liquid interface for 24 h in differentiation media (, followed by RNA harvest using the Aurum Total RNA Mini kit (Bio-Rad).

RNA-seq and analysis

For Figure S5, RNA from five scraped tracheas was pooled in duplicate experiments and submitted to the Vanderbilt Technologies for Advanced Genomics core for library preparation and RNA-seq. For Fig. 5 and Fig. S6, duplicate samples for each of the four genotype/expression conditions (n=8 total) were submitted to the HudsonAlpha Genomic Services Lab for library preparation and RNA-seq. For both experiments, reads were trimmed to remove adapter sequences with Flexbar v2.4 (Dodt et al., 2012) and aligned to mm10 using STAR (Dobin et al., 2013) v2.4.2a with GENCODE (Harrow et al., 2012) M7 comprehensive gene annotations. Cufflinks v2.1.1 (Roberts et al., 2011) was used to assemble transcripts and quantify their abundance. Cufflinks FPKM

estimates were converted to TPM estimates (Li et al., 2010) and are included in Supplementary Tables S2 and S4. For differential gene expression analysis, reads were assigned to GENCODE M7 comprehensive genes using featureCounts (Liao et al., 2014) (v1.4.6-p5) and tested for differential expression using DESeq2 (Love et al., 2014) v1.8.1 with default parameters. Genes with an adjusted p-value <0.1 in the DESeq2 output were considered significantly differentially expressed. Raw sequencing data have been deposited at the NCBI Sequence Read Archive under accession numbers SRA#X and SRA#X (will be given prior to publication).

ChIP-seq Data Analysis

Twenty to fifty million single-end 50 bp reads were generated for each ChIP-seq library using the Illumina HiSeq platform. Reads were trimmed to remove adapters sequences with Flexbar v2.4 (Dodt et al., 2012), aligned to GRCm38 using BWA-backtrack v0.6.1 (Li and Durbin, 2009) with default parameters, and filtered to remove reads with mapping qualities less than 30. MACS2 v2.0.10.20131216 (Zhang et al., 2008) was used to identify sites of genomic binding with default parameters and a q-value threshold of 0.05 using an input control. MACS2 binding sites were filtered to remove mouse ENCODE blacklisted regions (Consortium, 2012) and mitochondrial DNA sites. Annotation of binding sites with the nearest GENCODE M7 comprehensive TSS and overlap with genomic features was performed using Homer (Heinz et al., 2010) v4.7. Motif analysis was conducted using the GLAM2 (Frith et al., 2008) command line

tool. Correlation of read counts between ChIP-seq samples at sites of p63, p73, or Pol II genomic binding was performed with the deepTools bamCorrelate command line tool (Ramirez et al., 2014). The read alignments of ChIP-seq samples were 1X depth of coverage normalized for display in IGV using deepTools (Ramirez et al., 2014) bamCoverage command line tool. To analyze the overlap between our p73 ChIP-seq and the cilia-associated gene list, (Treutlein et al., 2014) we restricted our analysis to those genes shared between the different annotation methods used between the two studies.

References

Consortium, E.P. (2012). An integrated encyclopedia of DNA elements in the human genome. Nature *489*, 57-74.

Dobin, A., Davis, C.A., Schlesinger, F., Drenkow, J., Zaleski, C., Jha, S., Batut, P., Chaisson, M., and Gingeras, T.R. (2013). STAR: ultrafast universal RNA-seq aligner. Bioinformatics *29*, 15-21.

Dodt, M., Roehr, J.T., Ahmed, R., and Dieterich, C. (2012). FLEXBAR-Flexible Barcode and Adapter Processing for Next-Generation Sequencing Platforms. Biology *1*, 895-905.

Frith, M.C., Saunders, N.F., Kobe, B., and Bailey, T.L. (2008). Discovering sequence motifs with arbitrary insertions and deletions. PLoS computational biology *4*, e1000071.

Harrow, J., Frankish, A., Gonzalez, J.M., Tapanari, E., Diekhans, M., Kokocinski, F., Aken, B.L., Barrell, D., Zadissa, A., Searle, S.*, et al.* (2012). GENCODE: the reference human genome annotation for The ENCODE Project. Genome research *22*, 1760-1774.

Hayat, M.A. (1993). Stains and cytochemical methods (New York: Plenum Press).

Heinz, S., Benner, C., Spann, N., Bertolino, E., Lin, Y.C., Laslo, P., Cheng, J.X., Murre, C., Singh, H., and Glass, C.K. (2010). Simple combinations of lineage-determining transcription factors prime cis-regulatory elements required for macrophage and B cell identities. Molecular cell *38*, 576-589.

Lam, H.C., Choi, A.M., and Ryter, S.W. (2011). Isolation of mouse respiratory epithelial cells and exposure to experimental cigarette smoke at air liquid interface. Journal of visualized experiments : JoVE.

Li, B., Ruotti, V., Stewart, R.M., Thomson, J.A., and Dewey, C.N. (2010). RNA-Seq gene expression estimation with read mapping uncertainty. Bioinformatics *26*, 493-500.

Li, H., and Durbin, R. (2009). Fast and accurate short read alignment with Burrows-Wheeler transform. Bioinformatics *25*, 1754-1760.

Liao, Y., Smyth, G.K., and Shi, W. (2014). featureCounts: an efficient general purpose program for assigning sequence reads to genomic features. Bioinformatics *30*, 923-930.

Love, M.I., Huber, W., and Anders, S. (2014). Moderated estimation of fold change and dispersion for RNA-seq data with DESeq2. Genome biology *15*, 550.

Ramirez, F., Dundar, F., Diehl, S., Gruning, B.A., and Manke, T. (2014). deepTools: a flexible platform for exploring deep-sequencing data. Nucleic acids research *42*, W187-191.

Roberts, A., Pimentel, H., Trapnell, C., and Pachter, L. (2011). Identification of novel transcripts in annotated genomes using RNA-Seq. Bioinformatics *27*, 2325-2329.

Rosenbluth, J.M., Mays, D.J., Jiang, A., Shyr, Y., and Pietenpol, J.A. (2011). Differential regulation of the p73 cistrome by mammalian target of rapamycin reveals transcriptional programs of mesenchymal differentiation and tumorigenesis. Proceedings of the National Academy of Sciences of the United States of America *108*, 2076-2081.

Rosenbluth, J.M., Mays, D.J., Pino, M.F., Tang, L.J., and Pietenpol, J.A. (2008). A gene signature-based approach identifies mTOR as a regulator of p73. Molecular and cellular biology *28*, 5951-5964.

Rubinson, D.A., Dillon, C.P., Kwiatkowski, A.V., Sievers, C., Yang, L., Kopinja, J., Rooney, D.L., Zhang, M., Ihrig, M.M., McManus, M.T.*, et al.* (2003). A lentivirus-based system to functionally silence genes in primary mammalian cells, stem cells and transgenic mice by RNA interference. Nature genetics *33*, 401-406.

Treutlein, B., Brownfield, D.G., Wu, A.R., Neff, N.F., Mantalas, G.L., Espinoza, F.H., Desai, T.J., Krasnow, M.A., and Quake, S.R. (2014). Reconstructing lineage hierarchies of the distal lung epithelium using single-cell RNA-seq. Nature *509*, 371-375.

Vladar, E.K., and Brody, S.L. (2013). Analysis of ciliogenesis in primary culture mouse tracheal epithelial cells. Methods in enzymology *525*, 285-309.

Westfall, M.D., Mays, D.J., Sniezek, J.C., and Pietenpol, J.A. (2003). The Delta Np63 alpha phosphoprotein binds the p21 and 14-3-3 sigma promoters in vivo and has transcriptional repressor activity that is reduced by Hay-Wells syndrome-derived mutations. Molecular and cellular biology *23*, 2264-2276.

Zhang, Y., Liu, T., Meyer, C.A., Eeckhoute, J., Johnson, D.S., Bernstein, B.E., Nusbaum, C., Myers, R.M., Brown, M., Li, W.*, et al.* (2008). Model-based analysis of ChIP-Seq (MACS). Genome biology *9*, R137.